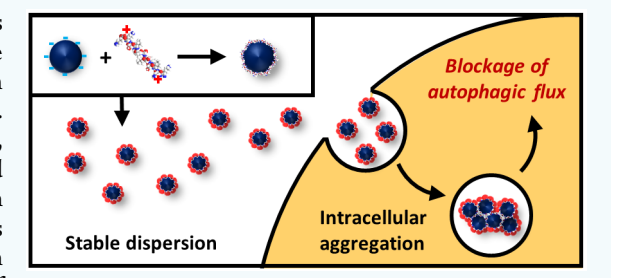


Aggregation Behavior of Nanoparticle-Peptide Systems Affects **Autophagy**

Santiago Martinez Legaspi[†] and Laura Segatori*, †,‡,§,||₀

Supporting Information

ABSTRACT: The aggregation of nanoparticle colloidal dispersions in complex biological environments changes the nanoparticle properties, such as size and surface area, thus affecting the interaction of nanoparticles at the interface with cellular components and systems. We investigated the effect of nanoparticle aggregation on autophagy, the main catabolic pathway that mediates degradation of nanosized materials and that is activated in response to internalization of foreign nanosized materials. We used carboxylated polystyrene nanoparticles (100 nm) and altered the nanoparticle aggregation behavior through addition of a multidomain peptide, thus generating a set of



nanoparticle-peptide mixtures with variable aggregation properties. Specifically, modulating the peptide concentration resulted in nanoparticle-peptide mixtures that are well dispersed extracellularly but aggregate upon cellular internalization. We monitored the effect of internalization of nanoparticle-peptide mixtures on a comprehensive set of markers of the autophagy pathway, ranging from transcriptional regulation to clearance of autophagic substrates. The nanoparticle-peptide mixtures were found to activate the transcription factor EB, a master regulator of autophagy and lysosomal biogenesis. We also found that intracellular aggregation of nanoparticle colloidal dispersions causes blockage of autophagic flux. This study provides important insights on the effect of the aggregation properties of nanoparticles on cells and, particularly, on the main homeostatic pathway activated in response to nanoparticle internalization. These results also point to the need to control the colloidal stability of nanoparticle systems for a variety of biomedical applications.

■ INTRODUCTION

Engineered nanoparticles have emerged as an important class of biomaterials for a variety of biomedical applications including delivery systems, 1,2 imaging and contrast agents, 2 and therapeutics.3 This wide range of applications is due to the unique and tunable physicochemical properties of nanoparticles that shape the interactions at the interface between nanoparticles and biological systems.^{4,5} Interactions at the nanobio interface, however, can also have bioadverse effects beyond those already characterized for materials at the bulk or molecular scales. 4,6,7 Specifically, mechanistic studies have pointed to the key role of nanoparticle-induced impairment and disruption of lysosomal function, formation of reactive oxygen species, and activation of inflammatory responses in mediating the observed cytotoxic effect of nanoparticles. Notably, the autophagic response induced upon internalization of a variety of nanoparticles presenting different physicochemical properties 11-16 has a profound effect on the fate of internalized nanoparticles and the ultimate outcome of the

interaction of nanoparticles with cellular components, including their potentially toxic effect. 17-20

Autophagy and, particularly, macroautophagy, is the main catabolic pathway in eukaryotic cells and plays a fundamental role in maintaining cell homeostasis.²¹ Activation of autophagy upon nanoparticle internalization may result in an increase in the cellular degradation capacity and enhanced clearance of endogenous materials. 12,13,15,22 However, nanoparticle internalization has also been linked to impairment of specific components of the autophagy-lysosome system.¹⁷ Impairment of this important homeostatic pathway has been associated with a variety of pathologies ranging from neurodegenerative diseases to cancer^{23,24} and may thus be involved in the mechanism of nanoparticle toxicity. Understanding the effect of nanoparticles on the autophagy system and mapping nanoparticle properties with the nature of the autophagic

Received: April 11, 2019 Revised: June 21, 2019 Published: June 24, 2019

Department of Chemical and Biomolecular Engineering, Rice University, 6100 Main Street, MS-362, Houston, Texas 77005, United States

[‡]Department of Bioengineering, Rice University, 6100 Main Street, MS-142, Houston, Texas 77005, United States

[§]Department of Biosciences, Rice University, 6100 Main Street, MS-140, Houston, Texas 77005, United States

Systems, Synthetic, and Physical Biology Graduate Program, Rice University, 6100 Main Street, MS-180, Houston, Texas 77005, United States

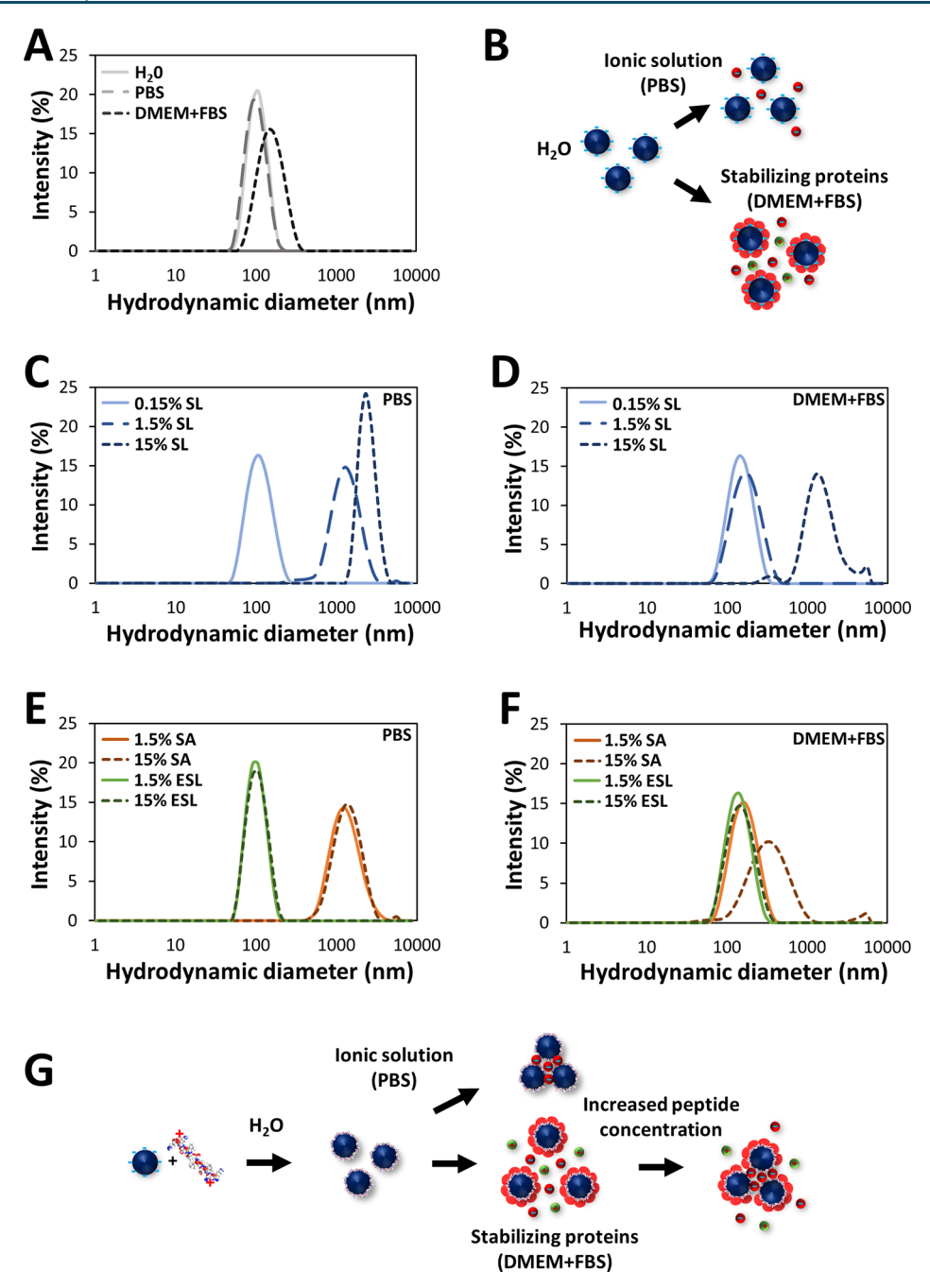


Figure 1. Hydrodynamic diameter size distributions of CPS-SL, CPS-SA, and CPS-ESL NPs. A) Hydrodynamic diameter distributions of 100 nm CPS NPs (50 μ g/mL) dispersed in water, PBS, and DMEM supplemented with FBS. B) Schematic representation of the colloidal behavior of CPS NPs. C, D) Hydrodynamic diameter distributions of CPS NPs mixed with SL peptide (0.15%, 1.5%, and 15% w/w peptide/NP) dispersed in C) PBS and in D) DMEM supplemented with FBS. E, F) Hydrodynamic diameter distributions of CPS NPs mixed with SA and ESL peptides (1.5% and 15% w/w peptide/NP) dispersed in E) PBS and in F) DMEM supplemented with FBS. G) Schematic representation of the colloidal behavior of CPS NP-peptide mixtures.

response elicited upon cellular internalization is thus important for the design of safe nanoparticles for use in biomedical applications. ²⁰

Autophagy mediates the degradation of aggregated proteins, damaged organelles, and pathogens through the lysosome. Clearance by the autophagy pathway initiates with compartmentalization of cytoplasmic material into double-membrane vesicles called autophagosomes. Autophagosomes fuse with lysosomes to form autolysosomes, and lysosomal hydrolases degrade the autophagic cargo. Autophagosome and lysosome biogenesis is regulated by the transcription factor EB (TFEB),

a master regulator that controls the expression of the CLEAR (coordinated lysosomal expression and regulation) gene network.²⁷ Interestingly, activation of autophagy upon internalization of different types of nanoparticles was found to correlate with activation of TFEB. ^{12,13,15,22} Upregulation of autophagy at the transcriptional level in cells exposed to nanoparticles, however, is not always paralleled by an increase in autophagic clearance. ^{13,15} Nanoparticles may disrupt components of the autophagy system: ¹⁷ lysosomal impairment induced by nanoparticles, for instance, leads to reduced

formation of autolysosomes, resulting in activation of TFEB paralleled by blockage of autophagic flux. 13,15,20

The high electrolyte and protein content of complex biological fluids affects the colloidal stability of nanoparticle systems, possibly causing nanoparticle aggregation.^{28–31} The intracellular milieu further affects the colloidal behavior of nanoparticles, especially upon nanoparticle exposure to the endolysosomal compartment.^{17,28} The colloidal stability and aggregation behavior of nanoparticles are expected to affect the nanoparticle physicochemical properties such as size, surface charge, and surface chemistry and are thus likely to play a key role in shaping the autophagic response to nanoparticles.^{11,13,32–34}

Most studies aimed at characterizing the impact of nanoparticles on cells as a function of nanoparticle aggregation have mainly focused on the aggregation behavior of nanoparticles in cell culturing media, which typically affects the rate and extent of cellular internalization of nanoparticles ³⁵ and is thus likely to shape the interaction of nanoparticles with intracellular components, including the autophagy pathway. ³⁶ The interaction of nanoparticles with intracellular components, however, may also alter the aggregation properties of nanoparticles upon cellular internalization and further affect the response of the autophagy system to nanoparticles. ¹⁴

In this study, we investigated the autophagic response to a nanoparticle-peptide system that presents peptide-dependent aggregation behavior in extracellular media as well as intracellularly. The nanoparticle-peptide system is based on carboxylated polystyrene nanoparticles which do not aggregate in cell culture media, 13 do not affect lysosomal function and stability,³⁷ and induce activation of autophagy without impairing components of the lysosome-autophagy system that mediate autophagic clearance. 13 By modulating the concentration of multidomain peptides with self-assembling properties, ^{38,39} we generated a set of NP-peptide mixtures with variable aggregation properties in extracellular media and intracellularly. Characterization of representative makers of the autophagy system, including transcriptional regulation, formation of autophagic vesicles, and cargo degradation, provided important insights on the impact of nanoparticles on autophagy as a function of nanoparticle colloidal behavior. Results from this study highlight the key role of the nanoparticle colloidal properties in shaping the autophagic response and will inform the design of safe nanoparticle systems with controlled properties at the interface with biological systems.

RESULTS AND DISCUSSION

The Aggregation Properties of NP-Peptide Mixtures Depend on the Ionic Strength and Protein Content of the Dispersant. To modulate the aggregation propensity of carboxylated polystyrene nanoparticles (CPS NPs), CPS NPs of 100 nm in diameter were mixed with the SL peptide ($K_2(SL)_6K_2$), a multidomain peptide that was previously reported to self-assemble into fibers in aqueous solution. The self-assembly properties of the SL peptide in solution are determined by the peptide's amino acid sequence and are affected by the solvent's pH and ionic strength. We expected the lysine residues at the N- and C-terminal ends of the peptide to be protonated at neutral pH and interact electrostatically with the carboxylic acid groups on the surface of the CPS NPs. We hypothesized that the aggregation propensity of CPS NPs coated with the SL peptide could be

modulated by varying the properties of the dispersant. Specifically, multivalent negative ions, which are present in buffers such as PBS, induce assembly of the peptide fibers into gels.³⁸ CPS NPs were mixed with the SL peptide (CPS-SL NPs) at 0.15%, 1.5%, and 15% w/w peptide/NP ratios. Dynamic light scattering (DLS) measurements revealed that the hydrodynamic diameter of CPS NPs does not vary between CPS NP dispersions in water and PBS (Figure 1A). The hydrodynamic diameter distribution of CPS NPs in serum-supplemented DMEM shifts slightly toward larger sizes, most likely due to the formation of the protein corona (Figure 1A). Results from DLS studies illustrate the colloidal stability of negatively charged nanoparticles in various dispersants (Figure 1B). The hydrodynamic diameter of CPS-SL NPs in water did not vary significantly as a function of peptide concentration (Figure S1A, Supporting Information). DLS measurements of CPS-SL NPs in PBS revealed an increase of 1 order of magnitude in the average hydrodynamic diameter of NP-peptide mixtures containing 1.5% and higher w/w peptide/NP ratios (Figure 1C), indicating that addition of the peptide alters the aggregation propensity of CPS NPs in an ionic solution such as PBS. The hydrodynamic diameter distributions of CPS SL NPs in serum-supplemented DMEM increased only in the mixture containing 15% SL (Figure 1D), indicating that the aggregation properties of NP-peptide mixtures depend on peptide concentration and are mediated by the protein content of the dispersant. This result is consistent with the notion that the protein corona enhances the colloidal stability of nanoparticles in biological fluids.³⁰

To further confirm the formation of aggregates in solution, we characterized the nanoparticle-peptide mixtures using nanoparticle tracking analysis (NTA), which allows visualization of the light scattered by nanoparticle suspensions and quantification of individual particle concentration and hydrodynamic size distribution. 41 Inspection of NTA videos shows well-defined and pointlike nanoparticle scattering signals for all nanoparticle-peptide mixtures in water (Figure S2A). Analyses of CPS NPs and 0.15% CPS-SL NPs in PBS also revealed welldefined pointlike scattering signals. Analyses of 1.5% and 15% CPS-SL NPs in PBS, however, revealed an increase in the size and intensity of the nanoparticle scattering signal and a decrease in the number of observed pointlike signals (Figure S2BC). The individual particle concentration of CPS NPs and CPS-SL NPs in PBS at 5 μ g/mL was found to be in the order of 10⁹ particles/mL. In contrast, the individual particle concentration of 1.5% and 15% CPS-SL NPs under the same conditions was found to be in the order of 10⁷ particles/mL, indicating aggregation of single particles. Analyses of the hydrodynamic size distributions of CPS-SL NPs (5 µg/mL in PBS) as a function of individual particle concentration show an increase in the hydrodynamic size distributions of the 1.5% and 15% CPS-SL NPs (Figure S2D).

To explore the role of the peptide sequence on the aggregation propensity of the nanoparticle-peptide mixtures, we analyzed CPS NPs mixed with other two multidomain peptides: $K_2(SL)_2(SA)_2(SL)_2K_2$ (SA peptide) and $E_2(SL)_6E_2$ (ESL peptide). Substitution of two leucine residues with two alanine residues in the SA peptide is expected to reduce the peptide's propensity to self-assemble; ³⁹ CPS-SA mixtures are thus expected to present reduced aggregation propensity. Substitution of the lysine residues with glutamate residues changes the electrostatic interactions between the particles, the peptides, and the ions in solution; CPS-ESL mixtures are thus

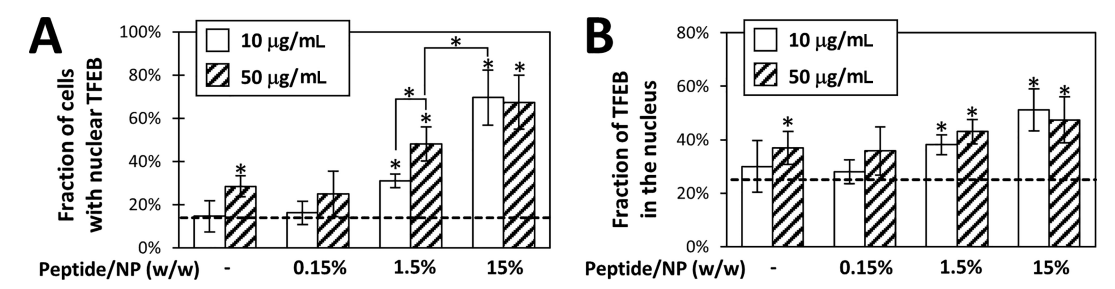


Figure 2. TFEB activation in HeLa/TFEB cells exposed to CPS-SL NPs. A) Average fraction of HeLa/TFEB cells treated with CPS NPs and CPS-SL NPs (10 and 50 μ g/mL; 24 h) that present nuclear localization of TFEB. Data reported as mean \pm SD ($n \ge 3$; $p \le 0.05$). B) Average fraction of TFEB that localizes to the nucleus of HeLa/TFEB cells treated with CPS NPs and CPS-SL NPs (10 and 50 μ g/mL; 24 h). Data reported as mean \pm SD ($n \ge 3$; $p \le 0.05$).

expected not to aggregate. CPS NPs were mixed with the SA and ESL peptides (CPS-SA and CPS-ESL NPs) at 1.5% and 15% w/w peptide/NP ratios because the CPS-SL NPs with those mixing ratios show aggregation in PBS and serumsupplemented DMEM. The hydrodynamic diameter of CPS-SA and CPS-ESL mixtures in water did not vary as a function of peptide sequence and concentration (Figure S1B). DLS measurements showed an increase in the average hydrodynamic diameter of CPS-SA NPs containing 1.5% and 15% SA in PBS (Figure 1E) and in serum-supplemented DMEM (Figure 1F). The aggregation behavior of 1.5% CPS-SA NPs is similar to that of 1.5% CPS-SL NPs. CPS-SA NPs containing 15% SA, however, do not aggregate to the extent observed in experiments conducted using CPS-SL NPs at the same mixing ratio. CPS-ESL NPs were found to not aggregate in any of the dispersants tested (Figure 1EF). These results confirm that the peptide sequence plays a key role in the aggregation properties of the CPS NPs coated with multidomain peptides.

These results suggest that the aggregation properties of CPS NPs can be controlled through addition of multidomain peptides. Specifically, we generated a set of NP-peptide mixtures, namely CPS NPs mixed with increasing concentrations of SL peptide (0, 0.15, 1.5, and 15% w/w peptide/NP ratios) with variable aggregation properties that depend on the nature of the dispersant (Figure 1G). Furthermore, because the aggregation properties of the NP-peptide mixtures in cell culture medium depend on the peptide concentration (Figure 1D), this nanoparticle preparation method allows exploring the effect of nanoparticle aggregation on the cellular response induced upon nanoparticle internalization.

Cell Exposure to NP-Peptide Mixtures Results in Activation of TFEB. To investigate the effect of the aggregation properties of the NP-peptide mixtures on the autophagy pathway, we first analyzed the transcriptional regulatory network that controls autophagy activation. Specifically, we monitored the transcription factor EB (TFEB), a master regulator of lysosomal biogenesis and autophagy that controls expression of genes of the CLEAR (coordinated lysosomal expression and regulation) network.⁴² TFEB resides predominantly in the cytoplasm of resting cells and translocates into the nucleus upon activation.²⁷ monitored the subcellular localization of TFEB in an in vitro model consisting of HeLa cells stably transfected for the expression of TFEB-3xFLAG (HeLa/TFEB cells).²⁷ HeLa/ TFEB cells were cultured in the presence of fluorescent CPS and CPS-SL NPs (10 and 50 μ g/mL; 24 h). TFEB subcellular localization was monitored by confocal microscopy using a Hoechst nuclear stain and an anti-FLAG antibody and

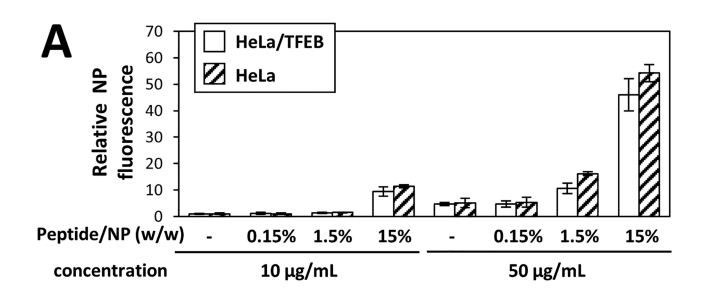
quantified by calculating the Mander's colocalization coefficient of the TFEB signal and the nuclear stain to determine the fraction of TFEB that localizes in the nucleus and the fraction of cells that present an increase in nuclear TFEB compared to untreated cells (Figure S3A). The average fraction of nuclear TFEB provides a measurement of the extent of TFEB activation per cell, whereas the average fraction of cells that present nuclear TFEB provides a measurement of the extent of TFEB activation within the cell population.

TFEB localizes predominantly in the cytoplasm of untreated cells (14% of cells with nuclear TFEB, Figure 2A, dashed line), as expected.²⁷ Cell treatment with CPS NPs (50 μ g/mL) induced a 2-fold increase in the fraction of cells with nuclear TFEB as previously reported¹³ ($p \le 0.05$; Figure 2A). Cell treatment with CPS-SL NPs resulted in an increase in the fraction of cells with nuclear TFEB compared to untreated cells and to cells treated with CPS NPs to an extent that depends on the concentration of SL peptide and on the concentration of CPS-SL NPs in the culturing medium. An increase in the fraction of cells with nuclear TFEB compared to untreated cells was observed in cells treated with CPS-SL NPs with at least 1.5% w/w peptide coating and at concentrations (10 μ g/mL) lower than the minimum concentration of CPS NPs that activates TFEB (50 μ g/mL) (1.5% SL NPs, $p \le 0.01$; 15% SL NPs, $p \le 0.001$; Figure 2A). The fraction of cells with nuclear TFEB increased with increasing concentration of CPS-SL NPs presenting 1.5% w/w peptide coating (50 μ g/mL) ($p \le 0.001$; Figure 2A). Treatment with 15% CPS-SL NPs was found to further increase the fraction of cells with nuclear TFEB (Figure 2A), but not in a concentration dependent fashion, possibly due to a plateau in the extent of the nanoparticle-induced effect on TFEB activity, as observed previously. 13 The fraction of TFEB that localizes to the nucleus in cells treated with CPS-SL NPs containing at least 1.5% SL was also found to increase compared to untreated cells and cells treated with CPS NPs, although it did not depend on the nanoparticle concentration in the medium (Figure 2B). Cell treatment with only the SL peptide at concentrations equivalent to the concentrations of peptide in CPS-SL NP treatments containing 15% SL was found to not increase the fraction of cells with nuclear TFEB or the fraction of TFEB in the nucleus (Figure S3BC).

These results demonstrate that cell treatment with CPS-SL NPs causes an increase in the fraction of cells that present nuclear TFEB and in the average fraction of TFEB that localizes to the nucleus compared to cells treated with CPS NPs, indicating an increase in the activation of TFEB that correlates with the relative amount of peptide in the NP-peptide mixture.

To determine whether addition of the multidomain peptides alters the cytotoxic properties of CPS NPs, we measured the viability of HeLa/TFEB cells treated with CPS-SL NPs using the MTS assay.⁴³ Treatment with CPS-SL NPs did not reduce cell viability under the conditions of this study (Figure S4).

To evaluate whether the SL peptide affects the uptake of NP-peptide mixtures, we measured the extent of CPS-SL NPs internalization as a function of the relative amount of peptide in the NP-peptide mixture and of CPS-SL NP concentration in the culturing medium. HeLa and HeLa/TFEB cells were treated with fluorescent CPS and CPS-SL NPs under conditions observed to induce changes in TFEB activation (10 and 50 μ g/mL; 24 h), and the extent of uptake was monitored by measuring cell fluorescence. Cellular uptake of CPS-SL NPs was similar in HeLa and HeLa/TFEB cells and depended on both amount of peptide and concentration of CPS-SL NPs (Figure 3A). Addition of 1.5% SL peptide



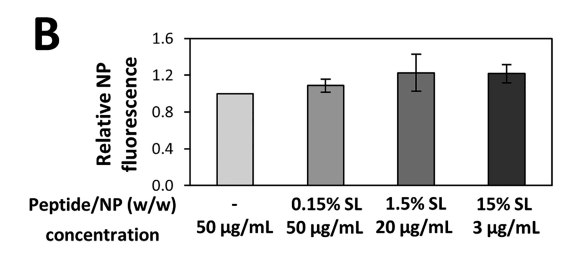


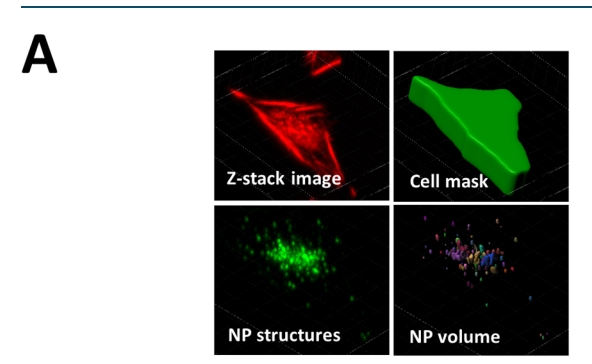
Figure 3. Uptake of CPS-SL NPs in HeLa/TFEB and HeLa cells. A) Average fluorescence of HeLa/TFEB and HeLa cells treated with fluorescent CPS NPs and CPS-SL NPs (10 and 50 μ g/mL; 24 h) normalized to the average fluorescence of cells treated with 10 μ g/mL CPS NPs. Data reported as mean \pm SD ($n \geq 3$). B) Average fluorescence of HeLa cells treated with fluorescent CPS NPs and CPS-SL NPs (at concentrations that result in comparable uptake) normalized to the average fluorescence of cells treated with 50 μ g/mL CPS NPs. Data reported as mean \pm SD ($n \geq 3$).

resulted in an increase in uptake only at high concentrations of NP-peptide mixtures (50 µg/mL) compared to CPS NPs not containing the peptide, while addition of 15% SL peptide resulted in an increase in uptake even at lower concentrations of NP-peptide mixtures in the medium (Figure 3A). The effect of the peptide coating on cellular uptake only partially explains the effect of the peptide coating on TFEB activation. For instance, cell treatment with low concentrations (10 μ g/mL) of CPS-SL NPs containing 1.5% SL resulted in similar uptake but higher TFEB activation compared to CPS NPs ($p \le 0.05$, Figure 2A). Furthermore, cell treatment with high concentrations (50 μ g/mL) of CPS-SL NPs containing 1.5% SL and low concentrations (10 μ g/mL) of CPS-SL NPs containing 15% SL resulted in comparable uptake levels but different effects on TFEB activation ($p \le 0.05$, Figure 2A). These results indicate that while the cellular internalization of CPS-

SL NPs correlates with the concentration of peptide coating and with the medium concentration of NP-peptide mixtures, the effect of CPS-SL NPs on TFEB activation does not depend solely on the extent of uptake of CPS-SL NPs.

To evaluate the extent to which the aggregation propensity of CPS-SL NPs affects the response of the autophagy pathway, we identified treatment conditions resulting in comparable cellular uptake of CPS NPs mixed with different amounts of SL peptide (normalized treatment concentrations, Figure 3B).

Intracellular Aggregation of NP-Peptide Mixtures. To determine whether the aggregation properties of the NPpeptide mixtures in saline buffer and cell culture media correlate with the extent of intracellular aggregation, we analyzed the formation of three-dimensional nanoparticle structures in single cells. HeLa cells were treated with CPS and CPS-SL NPs at concentrations that result in comparable uptake levels (normalized treatment concentrations, Figure 3B). Cells were analyzed by confocal microscopy, and threedimensional nanoparticle structures were constructed from stacks of confocal sections of single cells using the IMARIS software package (Figure 4A). The volume of each nanoparticle structure was determined based on the voxels defining the nanoparticle structure and the average nanoparticle structure volume calculated for each treatment condition. An increase in the average volume of intracellular NP structures with respect to cells treated with CPS NPs was observed in



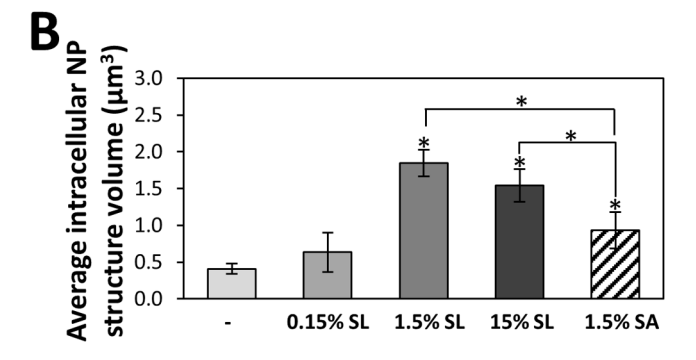


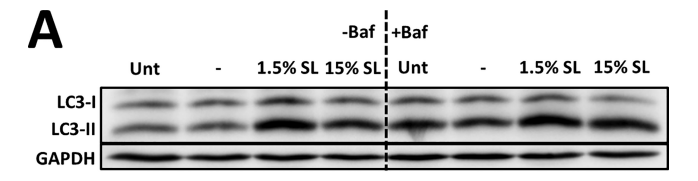
Figure 4. Nanoparticle aggregates in HeLa cells. A) Representative images used to measure intracellular nanoparticle structures in cells treated with fluorescent NPs. Single cell three-dimensional images are collected by confocal microscopy and analyzed using the IMARIS software package. The cell volume is determined using F-actin (red) and masked. The nanoparticle structures (green) inside the cell are analyzed based on voxel intensity to calculate the average nanoparticle structure volume. B) Average intracellular nanoparticle structure volume in cells treated with fluorescent CPS NPs, CPS-SL NPs, and CPS-SA NPs (normalized treatment concentrations; 24 h). Data reported as mean \pm SD ($n \ge 3$; $p \le 0.05$).

cells treated with CPS-SL NPs containing at least 1.5% SL peptide (4.5-fold; $p \le 0.001$) (Figure 4B). This result suggests that CPS NPs coated with multidomain peptides present enhanced aggregation propensity upon internalization into cells, since DLS analyses of NP-peptide mixtures in the culturing medium (Figure 1D) revealed increased aggregation only of CPS-SL NPs containing higher concentrations of peptides (15%). A comparison of DLS and intracellular aggregation analyses of CPS-SL NPs also supports this notion, as the size of nanoparticle aggregates was found to increase as a function of peptide concentration in samples of 1.5% and 15% CPS-SL NPs in extracellular medium (Figure 1D) but to plateau upon cellular internalization (Figure 4B). To determine the extent to which the peptide sequence influences the intracellular aggregation propensity of NP-peptide mixtures, we analyzed the formation of three-dimensional nanoparticle structures in single cells treated with CPS-SA NPs containing 1.5% SA peptide. CPS-SA NPs containing 1.5% SA were observed to present aggregation behavior similar to the 1.5% CPS-SL NPs in solution (Figure 1). Uptake analyses were first conducted to determine the normalized treatment concentration of 1.5% CPS-SA NPs (Figure S5BC). The increase in the average volume of intracellular NP structures in cells treated with 1.5% CPS-SA NPs with respect to cells treated with CPS NPs was considerably lower (2.3-fold; $p \le$ 0.005) than the increase in cells treated with 1.5% CPS-SL NPs, indicating that the peptide sequence affects the intracellular aggregation properties of the NP-peptide mixtures (Figure 4B).

Effect of NP-Peptide Mixture Aggregation on Autophagosome Synthesis and Turnover. Autophagic clearance involves a series of coordinated cellular processes, which include biogenesis of lysosomes and autophagosomes, fusion of lysosomes and autophagosomes, and formation of autolysosomes where degradation occurs.²⁶ To investigate the effect of NP-peptide mixtures with different aggregation properties on the autophagy pathway, we first evaluated the formation and turnover of autophagosomes under conditions that result in TFEB activation. Specifically, we measured the intracellular levels of microtubule-associated protein chain 3 (LC3) in HeLa cells treated with NP-peptide mixtures (normalized treatment concentrations, 24 h) by immunoblotting. 44 LC3 is a soluble cytoplasmic protein (LC3-I) that is conjugated to phosphatidylethanolamine (LC3-II) and recruited to autophagosomal membranes upon activation of autophagy. 45 Fusion of autophagosomes with lysosomes to form autolysosomes results in degradation of autophagosomal components including LC3-II. 46 The accumulation of LC3-II is thus indicative of autophagosome formation and turnover. 46

Cell treatment with NP-peptide mixtures containing at least 1.5% SL resulted in an increase in the levels of LC3-II compared to untreated cells (Figure 5B; $p \le 0.001$). Addition of the lysosomal protease inhibitor bafilomycin A1 (10 nM, 1 h) resulted in an increase in the LC3-II levels of untreated cells ($p \le 0.001$), cells treated with CPS NPs not containing peptide ($p \le 0.001$), and cells treated with NPs containing 0.15% SL ($p \le 0.005$; Figure 5B), due to blockage of autophagosome turnover caused by bafilomycin. However, addition of bafilomycin to cells treated with NP-peptide mixtures containing at least 1.5% SL did not affect LC3-II levels, indicating blockage of autophagic flux.

Taken together with the characterization of the extracellular (Figure 1) and intracellular (Figure 4) aggregation behavior of



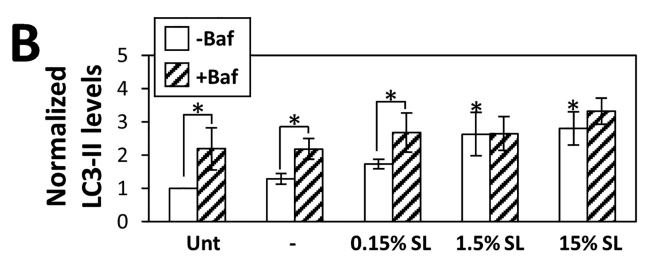


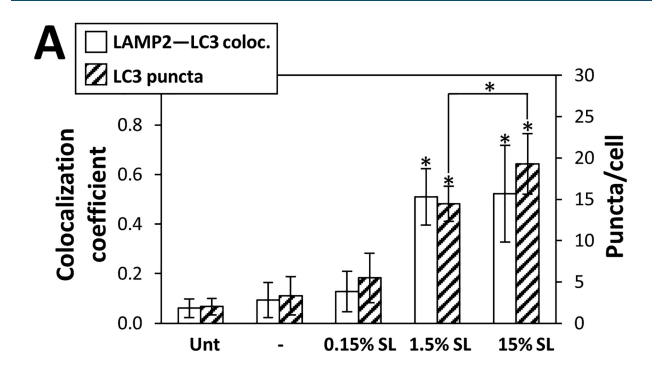
Figure 5. Autophagosome formation and turnover in HeLa cells exposed to CPS-SL NPs. LC3 levels in HeLa cells treated with CPS NPs and CPS-SL NPs (normalized treatment concentrations; 24 h) and in the presence of bafilomycin (10 nM; 1 h). A) Western blot analysis of LC3 isoforms (cytoplasmic LC3-I and autophagosome associated LC3-II). GAPDH is used as loading control. B) LC3-II band intensities, corrected by GAPDH band intensities, and normalized to the untreated sample. Data reported as mean \pm SD ($n \ge 3$; $p \le 0.05$).

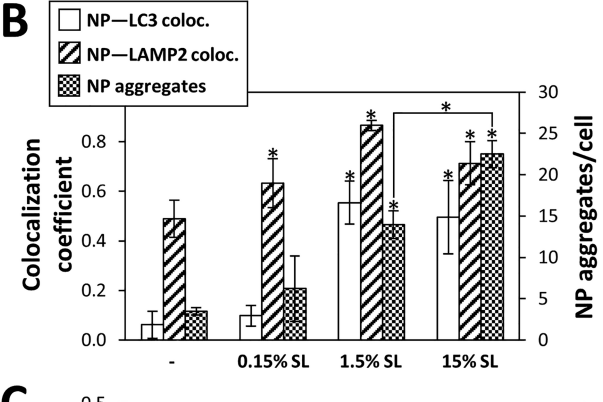
NP-peptide mixtures that form aggregated structures intracellularly causes blockage of the autophagic flux. Exposure to NP-peptide mixtures that form aggregated structures prior to NP-peptide mixtures that form aggregated structures prior to cellular uptake (15% SL NPs), on the other hand, did not affect the formation of autophagosomes. These results suggest that aggregation of NP-peptide mixtures that occur upon cellular uptake, rather than the intrinsic aggregation properties of the NP-peptide mixtures in the dispersing medium, affects the nature of the autophagic response elicited upon nanoparticle internalization.

Effect of NP-Peptide Mixture Aggregation on Lysosomal Integrity and Autophagic Flux. To further characterize the effect of CPS NP-peptide mixtures on the autophagic flux, we investigated the integrity of lysosomes and formation of autolysosomes. Lysosomal integrity was evaluated using acridine orange, a lysosomotropic probe with an emission spectrum that shifts from green to red as the probe accumulates in acidic organelles.⁴⁸ Lysosomal membrane permeabilization results in acridine orange release into the cytosol and decrease in red fluorescence. HeLa cells were treated with NP-peptide mixtures at the normalized treatment concentrations (24 h), and cell fluorescence was measured by flow cytometry. Cell treatment with CPS NPs did not affect lysosomal integrity as previously reported.¹³ Cell treatment with the NP-peptide mixtures did not affect the red fluorescence signal compared to cell treatment with CPS NPs (Figure S6), indicating that addition of the SL peptide does not affect lysosomal integrity.

To evaluate the effect of the NP-peptide mixtures on the autophagic flux, we also correlated LC3 processing to the formation of autolysosomes. HeLa cells were treated with NP-peptide mixtures (normalized treatment concentrations; 24 h) and autophagic vesicles evaluated using anti-LC3 and anti-LAMP2 (lysosome-associated membrane protein). Immunofluorescent confocal microscopy images were analyzed to quantify the number of LC3 puncta per cells and the extent of colocalization of LC3 and LAMP2 (Figure S7A). The average

number of LC3 puncta per cell increased in cells treated with at least 1.5% CPS-SL NPs compared to untreated cells ($p \le 0.001$; Figure 6A). This increase in LC3 puncta was paralleled





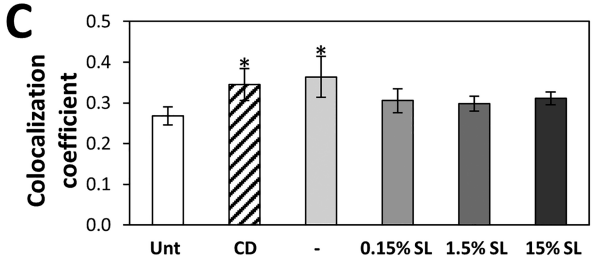


Figure 6. Autolysosome formation and ALR in HeLa cells exposed to CPS-SL NPs. A) Average number of LC3 puncta per cell and colocalization of LAMP2 with LC3 in HeLa cells treated with fluorescent CPS NPs and CPS-SL NPs (normalized treatment concentrations; 24 h). Data reported as mean \pm SD ($n \ge 3$; $p \le 0.05$). B) Average number of NP aggregates per cell and colocalization of NP aggregates with LC3 and LAMP2 in HeLa cells treated with fluorescent CPS NPs and CPS-SL NPs (normalized treatment concentrations; 24 h). Data reported as mean \pm SD ($n \ge 3$; $p \le 0.05$). C) Colocalization of CLTA with LAMP2 in HeLa cells treated with cyclodextrin (CD; 5 mM; 24 h) and fluorescent CPS NPs and CPS-SL NPs (normalized treatment concentrations; 24 h). Data reported as mean \pm SD ($n \ge 3$; $p \le 0.05$).

by an increase in LAMP2-LC3 colocalization ($p \le 0.001$; Figure 6A). Blockage of the autophagic flux that results from disruption of lysosomal integrity manifests as an increase in LC3 puncta that is not paralleled by an increase in LAMP2-LC3 colocalization. Because cells treated with CPS-SL NPs present an increase in LAMP2-LC3 colocalization, the blockage in autophagic flux observed in cells treated with CPS-SL NPs (Figure 5) is likely not to result from impairment of autolysosome formation. This observation is consistent with

analyses of acridine orange fluorescence indicating CPS-SL NPs do not affect lysosomal integrity (Figure S6). Cell treatment with only the SL peptide did not increase the average number of LC3 puncta or LAMP2-LC3 colocalization (Figure S7B).

To evaluate the localization of NP aggregates in autophagic vesicles, we quantified the colocalization of aggregated NP structures with protein markers of autophagosomes (LC3)⁴⁴ and lysosomes (LAMP2).50 HeLa cells were treated with the NP-peptide mixtures (normalized treatment concentrations; 24 h), and immunofluorescent confocal microscopy images were analyzed to quantify the number of NP aggregates per cell and the extent of colocalization of NPs with LC3 and LAMP2 (Figure S7A). We observed an increase in the average number of NP aggregates per cell in cells treated with at least 1.5% CPS-SL NPs compared to cells treated with CPS NPs ($p \le$ 0.001; Figure 6B). The increase in NP aggregates was paralleled by an increase in the colocalization of NP aggregates with autophagosomes ($p \le 0.001$; Figure 6B). CPS NPs were found to preferentially colocalize with lysosomes (Figure 6B), most likely due to the fusion of endosomes with lysosomes as the particles are internalized.¹⁷ We observed an increase in colocalization of NPs with lysosomes as a function of concentration of SL peptide even at low peptide concentrations compared to CPS NPs (0.15% SL, $p \le 0.01$), which was found to plateau at high peptide concentrations (Figure 6B). Taken together these results suggest that NP-peptide mixtures aggregate in lysosomes, most likely following internalization through the endolysosomal pathway. Disruption of the autophagic flux occurs after formation of autolysosomes, possibly due to impairment of autophagic lysosome reformation (ALR),⁵¹ an effect that has been reported for other biopersistent nanoparticles. 11,5

To determine the extent to which cells treated with the CPS NP-peptide mixtures present blockage of ALR, we monitored clathrin recruitment to autolysosomal membranes. Clathrin is recruited to autolysosomal membranes under conditions that activate autophagy.⁵³ Impairment of ALR, however, is not paralleled by an increase in recruitment of clathrin to autolysosomal membranes even in cells presenting an increase in accumulation of autolysosomes.⁵³ HeLa cells were treated with a known activator of autophagy, 22 cyclodextrin (CD; 5 mM; 24 h), and the NP-peptide mixtures (normalized treatment concentrations; 24 h). Immunofluorescent confocal microscopy images were analyzed to quantify the extent of colocalization of clathrin light chain A (CLTA) with LAMP2 (Figure S7C). As lysosomes and autophagosomes form autolysosomes, clathrin is recruited, and colocalization with LAMP2 increases. Treatment with cyclodextrin and CPS NPs resulted in an increase in CLTA-LAMP2 colocalization ($p \leq$ 0.01; Figure 6C). Treatment with CPS-SL NPs, however, did not result in an increase in CLTA-LAMP2 colocalization (Figure 6C). These results are consistent with the observation that CPS-SL NPs preferentially colocalize with lysosomes. As nanoparticles aggregate in lysosomes following internalization, the blockage of autophagic flux likely happens via impairment of ALR after the formation of autolysosomes.

We also observed that cells treated with CPS-SL NPs containing 15% SL peptide present an increase in the number of NP aggregates (Figure 6B) and LC3 puncta per cell (Figure 6A) compared to cells treated with 1.5% CPS-SL NPs ($p \le 0.05$) that was not paralleled by an increase in colocalization of NPs with autophagic vesicles. These results suggest that the

propensity of NP-peptide mixtures to form intracellular aggregates drives accumulation of NP aggregates within autophagic vesicles and affects the autophagic response to NPs. As a result, under comparable uptake of NP-peptide mixtures that aggregate extracellularly or intracellularly, formation of aggregates in the extracellular medium is likely to result in an increase in accumulation of aggregated structures compared to nanoparticles that only aggregate intracellularly but not to affect the extent to which NP aggregates accumulate in autophagic vesicles.

Intracellular Aggregation of NP-Peptide Mixtures Impairs Clearance of Autophagic Cargo. Pathological conditions characterized by blockage of autophagic flux lead to accumulation of autophagic cargo. 17,54 To test the extent to which the blockage of autophagic flux observed upon intracellular aggregation of NP-peptide mixtures affects autophagic clearance, we used an in vitro model of accumulation of autophagic cargo, namely fibroblasts derived from a patient with late infantile neuronal ceroid lipofuscinosis (LINCL). LINCL fibroblasts are characterized by accumulation of ceroid lipopigment, a lipofuscin-like autofluorescent material that is normally degraded through autophagy. 55 Cell treatment conditions resulting in comparable uptake of CPS and CPS-SL NPs in fibroblasts were first established (Figure S5D). LINCL fibroblasts were treated with fluorescent CPS and CPS-SL NPs (normalized treatment concentrations; 72 h), and intracellular aggregation was evaluated by confocal microscopy. The size of intracellular aggregates increased only in cells treated with 15% SL NPs ($p \le 0.01$; Figure 7A). The difference in the aggregation of NP-peptide mixtures upon cellular uptake between HeLa cells and LINCL cells is consistent with previous studies suggesting cell type dependent

To evaluate clearance of ceroid lipopigment, LINCL fibroblasts were treated with CPS and CPS-SL NPs

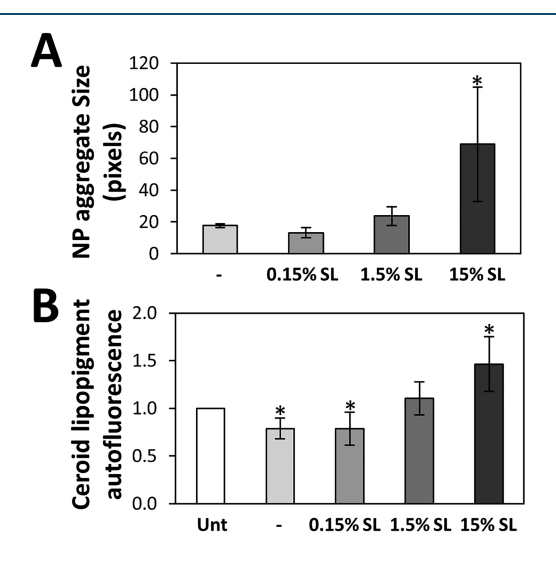


Figure 7. Clearance of ceroid lipopigment in LINCL fibroblasts exposed to CPS-SL and CPS-SA NPs. A) Two-dimensional intracellular aggregation analysis of LINCL fibroblasts treated with fluorescent CPS NPs and CPS-SL NPs (normalized treatment concentrations; 72 h). B) Ceroid lipopigment accumulation evaluated by quantifying the average mean pixel intensity in LINCL fibroblasts treated with CPS NPs and CPS-SL NPs (normalized treatment concentrations; 72 h) normalized by the average mean pixel intensity of untreated cells. Data reported as mean \pm SD ($n \ge 3$; $p \le 0.05$).

(normalized treatment concentrations; 72 h) and cell autofluorescence quantified using confocal microscopy. As expected, accumulation of ceroid lipopigment was reduced by 21% in cells treated with CPS NPs compared to untreated cells $(p \le 0.05; \text{ Figure 7B})$, which are known to induce activation of autophagy, resulting in enhanced clearance. 13 Treatment with NP-peptide mixtures resulted in a reduction in accumulation of ceroid lipopigment only in cells treated with 0.15% CPS-SL NPs (21%, $p \le 0.05$; Figure 7B). Treatment with 1.5% CPS-SL NPs did not affect the accumulation of ceroid lipopigment, and treatment with 15% CPS-SL NPs resulted in a 50% increase in the accumulation of ceroid lipopigment compared to untreated cells ($p \le 0.001$; Figure 7B). These results are consistent with the observation that NP-peptide mixtures that form aggregates upon cellular internalization (15% SL NPs, Figure 7A) cause blockage of the autophagic flux.

CONCLUSIONS

Nanoparticle colloidal dispersions are prone to aggregation in biological fluids.²⁸ In cell culture media commonly used for in vitro studies, electrolytes disrupt the repulsion caused by the electric double layer around nanoparticles, 29,31 while the high concentration of proteins can stabilize nanoparticle colloidal dispersions through the formation of the protein corona.^{29–31} Upon cellular internalization through the endolysosomal compartment, nanoparticles accumulate in a more complex environment characterized by more acidic pH.²⁸ Nanoparticle aggregation that occurs upon accumulation into the complex cellular milieu may affect the physicochemical properties of nanoparticle systems and the consequent cellular response. The autophagic response to nanoparticle internalization, which is potentially important in shaping the cytotoxic effect of nanoparticles, 17-20 seems to depend largely on the nanoparticle aggregation behavior. 14,36

In this study, we characterized the autophagic response to a NP-peptide mixture system (100 nm CPS NPs mixed with a multidomain peptide) 38,39 that presents peptide-dependent aggregation behavior. Cellular internalization of NP-peptide mixtures resulted in activation of TFEB in a peptide concentration-dependent fashion. Interestingly, formation of NP-peptide aggregates that occurred upon cellular internalization also resulted in blockage of autophagic flux. The NPpeptide aggregates were found to not disrupt lysosome integrity and autolysosome formation but to colocalize with autolysosomes, suggesting that intracellular aggregation of NPpeptide mixtures may increase nanoparticle biopersistence and that the observed disruption of autophagic flux may result from impairment of autophagic lysosome reformation. 11,51 Cellular internalization of NP-peptide mixtures that aggregate extracellularly is not followed by an increase in aggregation intracellularly and does not result in further blockage of autophagic flux. Finally, the observation that accumulation of autophagic cargo in an in vitro model system of lysosomal storage is exacerbated upon internalization of NP-peptide mixtures that aggregate intracellularly suggests that blockage of autophagic flux caused by formation of intracellular nanoparticle aggregates results in reduction in autophagic clearance. These results reconcile previously reported observations of the effect of nanoparticle aggregation on autophagy^{14,36} and underscore the need to evaluate colloidal stability in complex biological environments as part of the design of nanoparticles for biomedical applications.

MATERIALS AND METHODS

Nanoparticles and Cell Cultures. Carboxylated polystyrene nanoparticles (CPS NPs) were purchased from Magsphere (CA100NM, CAF100NM).

HeLa cells stably transfected to overexpress TFEB-3xFLAG (HeLa/TFEB) were a gift from Dr. Sardiello (Baylor College of Medicine).²⁷ Wild-type fibroblasts and fibroblasts derived from patients with late infantile neuronal ceroid lipofuscinosis (LINCL cells) were obtained from Coriell Cell Repositories (GM00498 and GM16486, respectively). HeLa cells (ATCC), HeLa/TFEB cells, wild-type fibroblasts, and LINCL cells were cultured using Dulbecco's Modified Eagle Medium (DMEM) supplemented with fetal serum albumin (FBS, 10% HeLa cells, 20% fibroblasts) and 1% penicillin-streptomycin-glutamine (PSQ). HeLa/TFEB cells were selected using G418 (1 mg/mL). LINCL cells were supplemented with 1X Non-Essential Amino Acids (NEAA, Lonza). Cells were cultured at 37 °C in 5% CO₂ and passaged using TrypLE Express.

NP-Peptide Mixtures Preparation and Characterization. SL and SA peptides were generously provided by Dr. Hartgerink (Rice University). NP-peptide mixtures (CPS-SL, CPS-SA) were prepared from 10 mg/mL suspensions of the CPS NPs in ultrapure DI water (18.2 M Ω -cm). The NP suspensions were mixed with varying amounts of a 3 mg/mL solution of peptide to an NP concentration of 5 mg/mL and w/w peptide/NP ratios of 0.15%, 1.5%, and 15%.

Particle hydrodynamic diameter measurements of NP-peptide mixtures were obtained with DLS using a Malvern Instruments Zen 3600 Zetasizer system. Stock suspensions of 5 mg/mL NPs in ultrapure water were probe sonicated for 30 s and diluted to an NP concentration of 50 μ g/mL in appropriate buffers.

NTA measurements were performed with a Malvern Instruments NanoSight NS 300 equipped with a 488 nm laser. Stock suspensions of 5 mg/mL NPs in ultrapure water were diluted to NP concentrations of 0.5 and 5 μ g/mL in appropriate buffers.

Cellular Uptake. The cellular uptake of the NP-peptide mixtures was measured by monitoring cell fluorescence using a fluorescence plate reader or a flow cytometer. Fluorescence plate reader measurements were obtained as previously described. Briefly, cells were seeded onto 96-well plates (5 × 10³ cells/well), treated with fluorescent NP-peptide mixtures for 24 h, washed with PBS, and incubated in acidic solution (50 mM glycine, 100 mM sodium chloride, 2 mg/mL polyvinylpyrrolidone (MW: 40k, pH 3) to remove NPs binding to the cell membrane as previously described. Cells were then washed with DI water and lysed with complete lysis-M buffer containing a protease inhibitor cocktail (Roche). The fluorescence intensity of the cell lysate was quantified using a SpectraMax Gemini plate reader (Molecular Device) (excitation 488 nm, emission 530 nm).

Flow cytometry measurements were conducted by seeding cells onto 12-well plates (6×10^4 HeLa cells/well, 10×10^4 fibroblasts/well). Cells were treated with fluorescent NP-peptide mixtures for 24 h, washed twice, and collected with PBS. Cell fluorescence was measured using a BD FACSCanto II flow cytometer with a 488 nm Argon laser and a 520 nm emission filter.

Cell Viability. Cells were seeded onto 96-well plates (4 \times 10³ cells/well) and treated with NP-peptide mixtures for 24 h. Cell viability was quantified using the CellTiter 96 Aqueous

One Solution Cell Proliferation Assay (Promega) according to the manufacturer's instructions.

Immunofluorescence. Immunofluorescence studies were conducted as previously described. ^{12,13} Briefly, cells were seeded as specified for each experiment, cultured in the presence of NP-peptide mixtures, and fixed with 4% paraformaldehyde (15 min) or 10% formaline (10 min) as indicated in each experiment. Cells were then permeabilized with 0.1% Triton X-100 (5 min) and incubated with 8% BSA in PBS (30 min). Images were obtained with a Nikon A-1 confocal microscope and the Nikon NIS Element C imaging software.

TFEB subcellular localization studies were conducted as previously described. 15 Briefly, HeLa/TFEB cells were seeded on glass coverslips in 24-well plates $(7.5 \times 10^3 \text{ cells/well})$, treated with fluorescent CPS-SL NPs for 24 h, and fixed with paraformaldehyde. Cells were incubated with anti-FLAG antibody (rabbit Sigma F7425; 1:1000) overnight at 4 °C, washed three times with 0.1% Tween-20 in PBS, and incubated with the secondary antibody (goat anti-rabbit Rockland 611-142-002; 1:500) for 2 h at room temperature. The nucleus was stained using a Hoechst nuclear stain. Image processing and colocalization analyses were conducted using the JACoP plugin⁶² in Fiji. ⁶³ The fraction of nuclear TFEB was quantified by calculating the Mander's colocalization coefficient (fraction of TFEB that colocalized with the Hoechst nuclear stain) for each image. The percentage of cells presenting TFEB nuclear localization was determined by calculating the number of cells displaying higher nuclear than cytoplasmic localization of

Colocalization of LC3 and LAMP and CLTA and LAMP was evaluated as previously described. 13,52 Briefly, HeLa cells were seeded on glass coverslips in 24-well plates (7.5×10^3) cells/well), incubated with fluorescent NP-peptide mixtures for 24 h, and fixed with paraformaldehyde. Cells were incubated overnight at 4 °C with primary antibodies (rabbit anti-LC3 Novus Biological NBP2-46892SS; 1:2000, or rabbit anti-CLTA Proteintech 10852-1-AP; 1:500, and mouse anti-LAMP-2 BioLegend 354301; 1:2000), washed three times with 0.1% Tween-20 in PBS, and incubated with appropriate secondary antibodies (goat anti-rabbit Rockland 611-142-002; 1:500 and goat anti-mouse KPL 072-05-18-06; 1:500) for 2 h at room temperature. The nucleus was stained using a Hoechst nuclear stain. Image processing and colocalization analyses were conducted using the JACoP plugin in Fiji. LC3-LAMP colocalization was quantified by calculating the Mander's colocalization coefficient (fraction of LAMP2 signal that colocalizes with LC3 signal) for each image. The number of LC3 puncta and number of NP aggregates per cell were determined by thresholding images and using the "analyze particles" function in Fiji. Colocalization of NP aggregates with LC3 and LAMP was quantified by calculating the Mander's colocalization coefficient (fraction of NP aggregates that colocalize with LC3 and LAMP) for each image.

For the analyses of intracellular NP aggregates, HeLa cells were seeded on glass coverslips in 24-well plates $(7.5\times10^3~{\rm cells/well})$, treated with fluorescent CPS-SL NPs for 24 h, and fixed with paraformaldehyde. Cells were incubated with anti-LC3 antibody (rabbit Novus Biological NB100-2220; 1:2000) overnight at 4 °C, washed three times with 0.1% Tween-20 in PBS, and incubated with secondary antibody (goat anti-rabbit Rockland 610-143-002; 1:500) for 2 h at room temperature. The cytoskeleton was stained using the ActinRed 555

ReadyProbes Reagent (Invitrogen). The volume of the threedimensional NP structures was determined by analyzing stacks of confocal sections of single cells using the IMARIS software package (Bitplane). The area of interest (cell) was manually defined using the cytoskeleton stain, and the analysis of NP structures was restricted to this area of interest by creating a mask. The surface detection tool was used to create 3D structures based on the fluorescence intensity of the NP signal. To select distinct NP structures above background fluorescence, the threshold of fluorescence intensity for the NP signal was determined using image stacks of cells treated with bare NPs (without peptide), and this threshold was applied to the analysis of all samples. The volume of each NP structure was calculated from the sum of positive voxels above the threshold.⁶⁴ The average volume of the in-cell 3D NP structures for each treatment condition was obtained from the mean volume of 3D structures in ≥ 10 cells per treatment from three biological replicates of each treatment.

To quantify NP aggregation and the accumulation of ceroid lipopigment in LINCL fibroblasts, fibroblasts were seeded on glass coverslips in 24-well plates (5×10^4 cells/well), treated with CPS-SL NPs for 72 h, and fixed with formaline. The nucleus was stained using the Hoechst nuclear stain. Image analysis was conducted using Fiji. The size of NP aggregates per cell was determined by thresholding images and using the "analyze particles" function in Fiji. The accumulation of ceroid lipopigment was quantified by calculating the average mean pixel intensity of at least 30 cells per sample in 8-bit images.

Western Blot Analyses. HeLa cells were seeded onto 10 mL dishes (60×10^4 cells/dish) and incubated with NP-peptide mixtures for 24 h. Cells were collected and lysed with complete lysis-M buffer containing a protease inhibitor cocktail (Roche). Total protein concentrations were determined using the Bradford assay, and 40 μg of protein from each sample was separated by 15% SDS-PAGE. Western blot analyses were conducted using primary antibodies (rabbit anti-LC3, Novus Biologics NB-100-2220; 1:1000 and mouse anti-GAPDH Santa Cruz Biotechnology sc-47724 1:5000) and appropriate secondary antibodies (anti-rabbit Santa Cruz Biotechnology sc-2004; 1:5000 and anti-mouse Santa Cruz Biotechnology sc-2005; 1:5000). Imaging was performed using a LAS 4000 Imager (Fujifilm), and relative band densities were determined using Fiji.

Lysosomal Integrity. Lysosomal integrity was analyzed using acridine orange as previously described. ⁴⁹ HeLa cells were seeded onto 12-well plates (6×10^4 cells/well), treated with NP-peptide mixtures for 24 h, and subsequently incubated with 5 μ g/mL acridine orange for 15 min. Samples were analyzed by flow cytometry using a 488 nm argon laser and 520 and 660 nm emission filters.

Statistical Analysis. All data are presented as mean \pm SD $(n \ge 3)$, and statistical significance was calculated using oneway analysis of variance followed by Dunnett's test for comparisons to untreated samples and the posthoc Tukey's test for comparisons between samples, unless stated otherwise.

ASSOCIATED CONTENT

Supporting Information

The Supporting Information is available free of charge on the ACS Publications website at DOI: 10.1021/acs.bioconjchem.9b00266.

Hydrodynamic diameter size distributions of CPS-SL, CPS-SA, and CPS-ESL NPs in water; NTA of CPS and CPS-SL NPs in water and in PBS; TFEB activation in HeLa/TFEB cells exposed to CPS-SL NPs and SL peptide; cytotoxicity of CPS-SL NPs; uptake of CPS-SL and CPS-SA NPs in HeLa/TFEB cells, HeLa cells, and fibroblasts; lysosomal integrity in HeLa cells exposed to CPS-SL NPs; colocalization of LC3, LAMP2, and nanoparticle aggregates, analysis of autolysosome formation, and colocalization of CLTA and LAMP2 in HeLa cells exposed to CPS-SL NPs and SL peptide (PDF)

AUTHOR INFORMATION

Corresponding Author

*E-mail: segatori@rice.edu. Phone: 713-348-3536. Corresponding author address: 6100 Main Street, MS-142, Houston, TX.

ORCID ®

Laura Segatori: 0000-0001-5749-5479

Notes

The authors declare no competing financial interest.

ACKNOWLEDGMENTS

This work was funded by the National Science Foundation (MCB-1615562 and 1150138 and CBET 1805317) and the Welch Foundation (C-1824). We would like to thank the Hartgerink Lab at Rice University for generously providing us the peptides used in this study.

ABBREVIATIONS

CPS NP, carboxylated polystyrene nanoparticle; TFEB, transcription factor EB; CLEAR, coordinated lysosomal expression and regulation; DLS, dynamic light scattering; NTA, nanoparticle tracking analysis; LC3, microtubule-associated protein chain 3; LAMP, lysosome-associated membrane protein; CLTA, clathrin light chain A; LINCL, late infantile neuronal ceroid lipofuscinosis

REFERENCES

- (1) Kim, B. Y. S., Rutka, J. T., and Chan, W. C. W. (2010) Nanomedicine. N. Engl. J. Med. 363, 2434–2443.
- (2) Bao, G., Mitragotri, S., and Tong, S. (2013) Multifunctional Nanoparticles for Drug Delivery and Molecular Imaging. *Annu. Rev. Biomed. Eng.* 15, 253–282.
- (3) Manthe, R. L., Foy, S. P., Krishnamurthy, N., Sharma, B., and Labhasetwar, V. (2010) Tumor Ablation and Nanotechnology. *Mol. Pharmaceutics* 7, 1880–1898.
- (4) Nel, A. E., Mädler, L., Velegol, D., Xia, T., Hoek, E. M. V., Somasundaran, P., Klaessig, F., Castranova, V., and Thompson, M. (2009) Understanding Biophysicochemical Interactions at the Nano–Bio Interface. *Nat. Mater.* 8, 543–557.
- (5) Albanese, A., Tang, P. S., and Chan, W. C. W. (2012) The Effect of Nanoparticle Size, Shape, and Surface Chemistry on Biological Systems. *Annu. Rev. Biomed. Eng.* 14, 1–16.
- (6) Elsaesser, A., and Howard, C. V. (2012) Toxicology of Nanoparticles. *Adv. Drug Delivery Rev.* 64, 129–137.
- (7) Sukhanova, A., Bozrova, S., Sokolov, P., Berestovoy, M., Karaulov, A., and Nabiev, I. (2018) Dependence of Nanoparticle Toxicity on Their Physical and Chemical Properties. *Nanoscale Res. Lett.* 13, 44.
- (8) Wang, J., Yu, Y., Lu, K., Yang, M., Li, Y., Zhou, X., and Sun, Z. (2017) Silica Nanoparticles Induce Autophagy Dysfunction via

Lysosomal Impairment and Inhibition of Autophagosome Degradation in Hepatocytes. *Int. J. Nanomed.* 12, 809–825.

- (9) Lee, Y.-H., Cheng, F.-Y., Chiu, H.-W., Tsai, J.-C., Fang, C.-Y., Chen, C.-W., and Wang, Y.-J. (2014) Cytotoxicity, Oxidative Stress, Apoptosis and the Autophagic Effects of Silver Nanoparticles in Mouse Embryonic Fibroblasts. *Biomaterials* 35, 4706–4715.
- (10) Lunov, O., Syrovets, T., Loos, C., Nienhaus, G. U., Mailander, V., Landfester, K., Rouis, M., and Simmet, T. (2011) Amino-Functionalized Polystyrene Nanoparticles Activate the NLRP3 Inflammasome in Human Macrophages. ACS Nano 5, 9648–9657.
- (11) Ma, X., Wu, Y., Jin, S., Tian, Y., Zhang, X., Zhao, Y., Yu, L., and Liang, X.-J. (2011) Gold Nanoparticles Induce Autophagosome Accumulation through Size-Dependent Nanoparticle Uptake and Lysosome Impairment. ACS Nano 5, 8629–8639.
- (12) Song, W., Soo Lee, S., Savini, M., Popp, L., Colvin, V. L., and Segatori, L. (2014) Ceria Nanoparticles Stabilized by Organic Surface Coatings Activate the Lysosome-Autophagy System and Enhance Autophagic Clearance. ACS Nano 8, 10328–10342.
- (13) Song, W., Popp, L., Yang, J., Kumar, A., Gangoli, V. S., and Segatori, L. (2015) The Autophagic Response to Polystyrene Nanoparticles Is Mediated by Transcription Factor EB and Depends on Surface Charge. *J. Nanobiotechnology* 13, 87.
- (14) Peynshaert, K., Soenen, S. J., Manshian, B. B., Doak, S. H., Braeckmans, K., De Smedt, S. C., and Remaut, K. (2017) Coating of Quantum Dots Strongly Defines Their Effect on Lysosomal Health and Autophagy. *Acta Biomater.* 48, 195–205.
- (15) Popp, L., Tran, V., Patel, R., and Segatori, L. (2018) Autophagic Response to Cellular Exposure to Titanium Dioxide Nanoparticles. *Acta Biomater.* 79, 354–363.
- (16) Popp, L., and Segatori, L. (2019) Zinc Oxide Particles Induce Activation of the Lysosome—Autophagy System. *ACS Omega 4*, 573—581.
- (17) Stern, S. T., Adiseshaiah, P. P., and Crist, R. M. (2012) Autophagy and Lysosomal Dysfunction as Emerging Mechanisms of Nanomaterial Toxicity. *Part. Fibre Toxicol.* 9, 20.
- (18) Zabirnyk, O., Yezhelyev, M., and Seleverstov, O. (2007) Nanoparticles as a Novel Class of Autophagy Activators. *Autophagy* 3, 278–281.
- (19) Peynshaert, K., Manshian, B. B., Joris, F., Braeckmans, K., De Smedt, S. C., Demeester, J., and Soenen, S. J. (2014) Exploiting Intrinsic Nanoparticle Toxicity: The Pros and Cons of Nanoparticle-Induced Autophagy in Biomedical Research. *Chem. Rev.* 114, 7581–7609
- (20) Popp, L., and Segatori, L. (2015) Differential Autophagic Responses to Nano-Sized Materials. *Curr. Opin. Biotechnol.* 36, 129–136.
- (21) Levine, B., and Klionsky, D. J. (2004) Development by Self-Digestion: Molecular Mechanisms and Biological Functions of Autophagy. *Dev. Cell* 6, 463–477.
- (22) Song, W., Wang, F., Lotfi, P., Sardiello, M., and Segatori, L. (2014) 2-Hydroxypropyl-β-Cyclodextrin Promotes Transcription Factor EB-Mediated Activation of Autophagy: Implications for Therapy. *J. Biol. Chem.* 289, 10211–10222.
- (23) Rubinsztein, D. C., Codogno, P., and Levine, B. (2012) Autophagy Modulation as a Potential Therapeutic Target for Diverse Diseases. *Nat. Rev. Drug Discovery* 11, 709–730.
- (24) Choi, A. M. K., Ryter, S. W., and Levine, B. (2013) Autophagy in Human Health and Disease. *N. Engl. J. Med.* 368, 651–662.
- (25) Wang, C.-W., and Klionsky, D. J. (2003) The Molecular Mechanism of Autophagy. *Mol. Med. 9*, 65–76.
- (26) Klionsky, D. J. (2007) Autophagy: From Phenomenology to Molecular Understanding in Less than a Decade. *Nat. Rev. Mol. Cell Biol.* 8, 931–937.
- (27) Sardiello, M., Palmieri, M., di Ronza, A., Medina, D. L., Valenza, M., Gennarino, V. A., Di Malta, C., Donaudy, F., Embrione, V., Polishchuk, R. S., et al. (2009) A Gene Network Regulating Lysosomal Biogenesis and Function. *Science* 325, 473–477.
- (28) Moore, T. L., Rodriguez-Lorenzo, L., Hirsch, V., Balog, S., Urban, D., Jud, C., Rothen-Rutishauser, B., Lattuada, M., and Petri-

Fink, A. (2015) Nanoparticle Colloidal Stability in Cell Culture Media and Impact on Cellular Interactions. *Chem. Soc. Rev.* 44, 6287–6305.

- (29) Mahl, D., Greulich, C., Meyer-Zaika, W., Köller, M., and Epple, M. (2010) Gold Nanoparticles: Dispersibility in Biological Media and Cell-Biological Effect. *J. Mater. Chem.* 20, 6176–6181.
- (30) Gebauer, J. S., Malissek, M., Simon, S., Knauer, S. K., Maskos, M., Stauber, R. H., Peukert, W., and Treuel, L. (2012) Impact of the Nanoparticle–Protein Corona on Colloidal Stability and Protein Structure. *Langmuir* 28, 9673–9679.
- (31) Ji, Z., Jin, X., George, S., Xia, T., Meng, H., Wang, X., Suarez, E., Zhang, H., Hoek, E. M. V., Godwin, H., et al. (2010) Dispersion and Stability Optimization of TiO 2 Nanoparticles in Cell Culture Media. *Environ. Sci. Technol.* 44, 7309–7314.
- (32) Wick, P., Manser, P., Limbach, L. K., Dettlaff-Weglikowska, U., Krumeich, F., Roth, S., Stark, W. J., and Bruinink, A. (2007) The Degree and Kind of Agglomeration Affect Carbon Nanotube Cytotoxicity. *Toxicol. Lett.* 168, 121–131.
- (33) Zhang, Y., Zheng, F., Yang, T., Zhou, W., Liu, Y., Man, N., Zhang, L., Jin, N., Dou, Q., Zhang, Y., et al. (2012) Tuning the Autophagy-Inducing Activity of Lanthanide-Based Nanocrystals through Specific Surface-Coating Peptides. *Nat. Mater.* 11, 817–826.
- (34) Wu, L., Zhang, Y., Zhang, C., Cui, X., Zhai, S., Liu, Y., Li, C., Zhu, H., Qu, G., Jiang, G., et al. (2014) Tuning Cell Autophagy by Diversifying Carbon Nanotube Surface Chemistry. *ACS Nano 8*, 2087–2099.
- (35) Albanese, A., and Chan, W. C. W. (2011) Effect of Gold Nanoparticle Aggregation on Cell Uptake and Toxicity. *ACS Nano 5*, 5478–5489.
- (36) Huang, D., Zhou, H., and Gao, J. (2015) Nanoparticles Modulate Autophagic Effect in a Dispersity-Dependent Manner. *Sci. Rep.* 5, 14361.
- (37) Fröhlich, E., Meindl, C., Roblegg, E., Ebner, B., Absenger, M., and Pieber, T. R. (2012) Action of Polystyrene Nanoparticles of Different Sizes on Lysosomal Function and Integrity. *Part. Fibre Toxicol.* 9, 26.
- (38) Aulisa, L., Dong, H., and Hartgerink, J. D. (2009) Self-Assembly of Multidomain Peptides: Sequence Variation Allows Control over Cross-Linking and Viscoelasticity. *Biomacromolecules* 10, 2694–2698.
- (39) Li, I.-C., Moore, A. N., and Hartgerink, J. D. (2016) Missing Tooth" Multidomain Peptide Nanofibers for Delivery of Small Molecule Drugs. *Biomacromolecules* 17, 2087–2095.
- (40) Dong, H., Paramonov, S. E., Aulisa, L., Bakota, E. L., and Hartgerink, J. D. (2007) Self-Assembly of Multidomain Peptides: Balancing Molecular Frustration Controls Conformation and Nanostructure. *J. Am. Chem. Soc.* 129, 12468–12472.
- (41) Filipe, V., Hawe, A., and Jiskoot, W. (2010) Critical Evaluation of Nanoparticle Tracking Analysis (NTA) by NanoSight for the Measurement of Nanoparticles and Protein Aggregates. *Pharm. Res.* 27, 796–810.
- (42) Settembre, C., Di Malta, C., Polito, V. A., Arencibia, M. G., Vetrini, F., Erdin, S., Erdin, S. U., Huynh, T., Medina, D., Colella, P., et al. (2011) TFEB Links Autophagy to Lysosomal Biogenesis. *Science (Washington, DC, U. S.)* 332, 1429–1433.
- (43) Buttke, T. M., McCubrey, J. A., and Owen, T. C. (1993) Use of an Aqueous Soluble Tetrazolium/Formazan Assay to Measure Viability and Proliferation of Lymphokine-Dependent Cell Lines. *J. Immunol. Methods* 157, 233–240.
- (44) Mizushima, N., Yoshimori, T., and Levine, B. (2010) Methods in Mammalian Autophagy Research. *Cell* 140, 313–326.
- (45) Kabeya, Y., Mizushima, N., Ueno, T., Yamamoto, A., Kirisako, T., Noda, T., Kominami, E., Ohsumi, Y., and Yoshimori, T. (2000) LC3, a Mammalian Homologue of Yeast Apg8p, Is Localized in Autophagosome Membranes after Processing. *EMBO J.* 19, 5720–5728
- (46) Tanida, I., Minematsu-Ikeguchi, N., Ueno, T., and Kominami, E. (2005) Lysosomal Turnover, but Not a Cellular Level, of Endogenous LC3 Is a Marker for Autophagy. *Autophagy* 1, 84–91.

(47) Rubinsztein, D. C., Cuervo, A. M., Ravikumar, B., Sarkar, S., Korolchuk, V. I., Kaushik, S., and Klionsky, D. J. (2009) In Search of an "Autophagomometer. *Autophagy 5*, 585–589.

- (48) Han, J., and Burgess, K. (2010) Fluorescent Indicators for Intracellular PH. Chem. Rev. 110, 2709-2728.
- (49) Yuan, X.-M., Li, W., Dalen, H., Lotem, J., Kama, R., Sachs, L., and Brunk, U. T. (2002) Lysosomal Destabilization in P53-Induced Apoptosis. *Proc. Natl. Acad. Sci. U. S. A.* 99, 6286–6291.
- (50) Eskelinen, E.-L., Tanaka, Y., and Saftig, P. (2003) At the Acidic Edge: Emerging Functions for Lysosomal Membrane Proteins. *Trends Cell Biol.* 13, 137–145.
- (51) Yu, L., McPhee, C. K., Zheng, L., Mardones, G. A., Rong, Y., Peng, J., Mi, N., Zhao, Y., Liu, Z., Wan, F., et al. (2010) Termination of Autophagy and Reformation of Lysosomes Regulated by MTOR. *Nature* 465, 942–946.
- (52) Zhang, J.-Q., Zhou, W., Zhu, S.-S., Lin, J., Wei, P.-F., Li, F.-F., Jin, P.-P., Yao, H., Zhang, Y.-J., Hu, Y., et al. (2017) Persistency of Enlarged Autolysosomes Underscores Nanoparticle-Induced Autophagy in Hepatocytes. *Small* 13, 1602876.
- (53) Rong, Y., Liu, M., Ma, L., Du, W., Zhang, H., Tian, Y., Cao, Z., Li, Y., Ren, H., Zhang, C., et al. (2012) Clathrin and Phosphatidylinositol-4,5-Bisphosphate Regulate Autophagic Lysosome Reformation. *Nat. Cell Biol.* 14, 924–934.
- (54) Levine, B., and Kroemer, G. (2008) Autophagy in the Pathogenesis of Disease. *Cell* 132, 27–42.
- (55) Kohlschütter, A., and Schulz, A. (2009) Towards Understanding the Neuronal Ceroid Lipofuscinoses. *Brain Dev.* 31, 499–502.
- (56) Olivier, V., Rivière, C., Hindié, M., Duval, J.-L., Bomila-Koradjim, G., and Nagel, M.-D. (2004) Uptake of Polystyrene Beads Bearing Functional Groups by Macrophages and Fibroblasts. *Colloids Surf.*, B 33, 23–31.
- (57) Lorenz, M. R., Holzapfel, V., Musyanovych, A., Nothelfer, K., Walther, P., Frank, H., Landfester, K., Schrezenmeier, H., and Mailänder, V. (2006) Uptake of Functionalized, Fluorescent-Labeled Polymeric Particles in Different Cell Lines and Stem Cells. *Biomaterials* 27, 2820–2828.
- (58) Johnston, H. J., Semmler-Behnke, M., Brown, D. M., Kreyling, W., Tran, L., and Stone, V. (2010) Evaluating the Uptake and Intracellular Fate of Polystyrene Nanoparticles by Primary and Hepatocyte Cell Lines in Vitro. *Toxicol. Appl. Pharmacol.* 242, 66–78.
- (59) Firdessa, R., Oelschlaeger, T. A., and Moll, H. (2014) Identification of Multiple Cellular Uptake Pathways of Polystyrene Nanoparticles and Factors Affecting the Uptake: Relevance for Drug Delivery Systems. *Eur. J. Cell Biol.* 93, 323–337.
- (60) Xu, A., Yao, M., Xu, G., Ying, J., Ma, W., Li, B., and Jin, Y. (2012) A Physical Model for the Size-Dependent Cellular Uptake of Nanoparticles Modified with Cationic Surfactants. *Int. J. Nanomedicine* 7, 3547–3554.
- (61) Hassan, A. A., Chan, B. T.-Y., Tran, L. A., Hartman, K. B., Ananta, J. S., Mackeyev, Y., Hu, L., Pautler, R. G., Wilson, L. J., and Lee, A. V. (2010) Serine-Derivatized Gadonanotubes as Magnetic Nanoprobes for Intracellular Labeling. *Contrast Media Mol. Imaging 5*, 34–38.
- (62) Bolte, S., and Cordelieres, F. P. (2006) A Guided Tour into Subcellular Colocalisation Analysis in Light Microscopy. *J. Microsc.* 224, 213–232.
- (63) Schindelin, J., Arganda-Carreras, I., Frise, E., Kaynig, V., Longair, M., Pietzsch, T., Preibisch, S., Rueden, C., Saalfeld, S., Schmid, B., et al. (2012) Fiji: An Open-Source Platform for Biological-Image Analysis. *Nat. Methods* 9, 676–682.
- (64) Cho, H.-J., Robinson, E. S., Rivera, L. R., McMillan, P. J., Testro, A., Nikfarjam, M., Bravo, D. M., and Furness, J. B. (2014) Glucagon-like Peptide 1 and Peptide YY Are in Separate Storage Organelles in Enteroendocrine Cells. *Cell Tissue Res.* 357, 63–69.